

A catalog of multi-vantage point observations of type-II bursts: Statistics and correlations

Atul Mohan^{1,2}, Nat Gopalswamy¹, Hemapriya Raju³ and Sachiko Akiyama^{1,2}

¹NASA Goddard Space Flight Center, 8800 Greenbelt Road Greenbelt, MD, 20771, USA

²The Catholic University of America, 620 Michigan Avenue, N.E. Washington, DC 20064, USA

³Indian Institute of Technology, Indore, Simrol, Indore, 453552, India

Abstract. Coronal mass ejection (CME) often produces a soft X-ray (SXR) flare associated with the low-coronal reconnection and a type-II radio burst associated with an interplanetary (IP) CME-shock. SXR flares and type-II bursts outshine the background emission, making them sun-as-a-star observables. Though there exist SXR flare catalogs covering decades of observations, they do not provide the associated type-II luminosity. Besides, since radio burst emission could be beamed, the observed flux dynamic spectrum may vary with line of sight. Using long-term calibrated decameter-hectometric dynamic spectra from the Wind and STEREO spacecraft, we build a catalog of multi-vantage point observations of type-II bursts. Cross-matching with existing catalogs we compile the properties of the associated flare, reconnection, and the CME. Cross-correlation analysis was done between various parameters. Two novel metrics of flare and CME power show a strong correlation revealing a link between particle acceleration strengths in the low corona and IP space.

Keywords. Solar coronal mass ejections, Catalogs, Stellar coronal mass ejections

1. Introduction

Solar coronal mass ejections (CMEs) are a major driver of energetic space weather phenomena, like solar energetic particle events (SEPs), geomagnetic storms etc. CMEs are often associated with flares across the electromagnetic spectrum, from radio to gamma-rays (see, [Howard et al. 2023](#), for an overview). The two major processes during a flare-CME event include the reconnection event that accelerates electrons leading to the SXR flare in the low corona, and the CME shock that accelerates particles across the corona and interplanetary space often leading to type-II radio bursts (e.g. [Wild & McCready 1950](#); [McLean & Labrum 1985](#); [Gopalswamy 2011](#)) in meter - kilometer (m-km) band. [Gopalswamy et al. \(2018b\)](#) showed that the low coronal flare-reconnection flux, ϕ_{rec} , correlates well with the CME kinetic energy revealing a link between the strengths of the low coronal and interplanetary impacts of the active phenomenon. However, despite decades of observations, we lack an understanding of the relationships, if any, between the observational proxies to the strengths of the particle acceleration in the low corona (peak SXR luminosity, L_X) and interplanetary space (peak type-II luminosity, L_R), and the physical properties of their drivers (i.e., flare and CME).

Meanwhile, when it comes to stellar CMEs, unlike the solar case, spatially resolved observations are impossible with current telescopes limiting the capability to directly infer crucial physical parameters, particularly ϕ_{rec} and CME speed (V_{CME}). Hence, scaling laws linking sun-as-a-star L_X and L_R , to relevant spatially resolved physical properties are important to constrain stellar CME models and to understand the solar-stellar flare-CME phenomenon within a common framework. There exist SXR flare and CME catalogs, that report L_X , ϕ_{rec} (in some cases), V_{CME} etc. for decades of solar-CME observations, but they do not report simultaneous L_R for any associated type-II bursts. Besides, m - km burst emission is inherently beamed

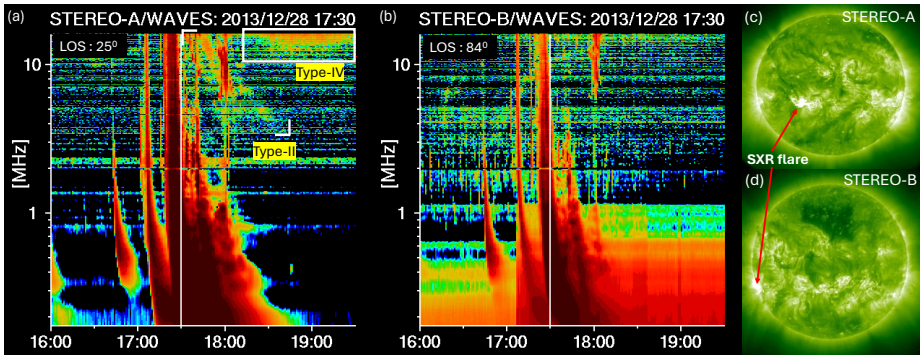


Figure 1. (a-b): DH DS from STEREO-A and B during a CME. The associated active region was at 25° and 84° lines of sight (LOS) in respective spacecraft. The type-II (marked by angular brackets) and type-IV (marked by box) seen in STEREO-A DS is absent in STEREO-B data. (c-d) The 195\AA images from both spacecraft show the SXR flare, marked by arrows.

as demonstrated for different burst types (e.g. Dulk et al. 1980; Gopalswamy 2011; Saint-Hilaire et al. 2013; Mohan et al. 2024). Apart from inherent directivity, the line of sight (LOS) plasma and magnetic field structures can also impact the observed emission characteristics in the dynamic spectrum (DS) (e.g. Robinson & Cairns 1994; Arzner & Magun 1999; Talebpour Sheshvan & Pohjolainen 2018). Figure 1 shows an event observed by STEREO-A and STEREO-B spacecraft with the flaring active region at 25° and 84° lines of sight (LOS) respectively. The decameter-hectometric (DH) DS and the X-ray images from both spacecraft are compared. STEREO-A spacecraft observed the frequency drifting type-II burst and the long-duration stationary type-IV emission confined above 10 MHz (see, McLean & Labrum 1985, for an overview of the burst types). Clearly, STEREO-B does not observe both type-II and type-IV bursts, though both spacecraft see the SXR flare. Hence the LOS towards the active latitudes on the star can be crucial in choosing a target star with a high chance of detecting a radio burst. The first step to performing such detailed studies of the properties of the observed type-II bursts is to build a comprehensive catalog of multi-vantage point observations of type-II bursts listing their spectro-temporal properties and L_R , and the properties of the associated flares and CMEs. We present such a catalog and the initial results on the correlations between various parameters.

2. Data and event catalog

The calibrated DH band dynamic spectra recorded by Plasma Wave Investigation (WAVES) instruments onboard Wind, STEREO-A and STEREO-B spacecraft since Nov 2006 form a unique uniformly calibrated multi-vantage point dataset ideal for the goals of the study. This long-term database spans two solar cycles and the rising phase of the current cycle. The other aspects that make DH bursts interesting are the following. DH type-IIs are associated with interplanetary shocks driven by energetic CMEs. In the stellar CME studies, despite hours and days-long searches on stars with very high flaring rates in the meterwave band, not a single type-II burst has been found (e.g. Bastian 1990; Osten & Bastian 2008; Crosley & Osten 2018; Villadsen & Hallinan 2019). Numerical simulations suggest that due to the strong magnetic fields in the atmospheres of active stars, an eruptive event may not be able to generate shocks in the lower corona but probably at interplanetary heights, favoring DH band over the meterwave band (Odert et al. 2020; Alvarado-Gómez et al. 2022). Also, compared to their metric counterparts, the DH type-II bursts are associated with relatively stronger flares and faster

DH type-II													Associated events									
Properties						Quality metrics						CME				Flare			SEP			
Start_date	Start_time	End_date	End_time	Freq_start	Freq_end	Detection	Best Mission	Peak Flux (log SFU)	F_thresh (log SFU)	Data	Event	Reliability	CME_date	CME_time	Width	Speed	Src_loc	NOAA	GOES	Rec_flux	IBI	Flux (>10 MeV)
UT	UT	UT	UT	kHz	kHz								UT	UT	deg	km/s				Mx	G	cm ² s ⁻¹ sr ⁻¹
2011/02/15	02:10	2011/02/15	07:00	16000	400	Wind.STA.STB	Wind	6.1	3.7	W2A2B2	S3I3	FOR1	2011/02/15	02:24	360	669	S20W12	11158	X2.2	6.47e+21	286.0	nan
2011/06/02	06:00	2011/06/02	06:25	15000	4000	Wind.STB	STB	3.7	2.4	W2A2B2	S2I2	FOR1	2011/06/02	08:12	360	976	S19E25	11227	C3.7	9.59e+20	63.0	nan
2012/01/19	15:00	2012/01/20	02:45	16000	100	STA.STB.Wind	Wind	4.2	3.7	W2A2B2	S3I3	FOR1	2012/01/19	14:36	360	1120	N32E22	11402	M3.2	4.4e+21	443.0	nan
2012/03/10	17:55	2012/03/11	12:30	14000	300	STA.Wind	STA	4.25	2.6	W2A2B2	S2I2	FOR1	2012/03/10	18:00	360	1296	N17W24	11429	M8.4	7.86e+21	276.0	nan
2013/05/13	16:15	2013/05/13	19:10	8000	300	Wind.STA.STB	STB	5.7	2.4	W2A2B2	S3I3	FOR1	2013/05/13	16:07	360	1850	N11E85	11748	X2.8	6.42E+20	3	nan
2013/09/29	21:53	2013/09/30	21:00	14000	60	Wind.STA	Wind	4.8	3.7	W2A2B2	S2I3	FOR1	2013/09/29	22:12	360	1179	N17W29	EP	C1.3	3.48e+21	10.0	nan
2013/10/26	03:01	2013/10/26	04:00	14000	1800	Wind.STA	Wind	4.3	3.7	W2A2B2	S2I2	FOR1	2013/10/26	03:12	208	473	N09W44	11875	C4.5	3.93e+20	332.0	nan

Figure 2. A portion of List 2, that presents DH type-II events with reliable L_R, L_X, ϕ_{rec} and V_{CME} estimates. Refer text for details. All event lists and their description can be found at https://cdaw.gsfc.nasa.gov/CME_list/radio/multimission_type2/.

CMEs (Gopalswamy 2011; Miteva et al. 2017). The DH type-II bursts are also strongly associated with SEPs and solar gamma-ray events making them more space weather relevant (Miteva et al. 2017; Gopalswamy et al. 2018c).

2.1. The multi-vantage point flare- CME- type-II catalog

The initial list of DH type-II bursts comes from Gopalswamy et al. (2019). For each event, we assign a ‘data quality’ metric based on the quality of the data from each spacecraft. The data quality metric is of the form $W_xA_yB_z$, where $x, y, z \in 0, 1, 2$. W stands for Wind, A for STEREO-A and B for STEREO B, while the integer metric attached conveys the quality of the data stream. When 0 represents data gap, 1 represents a poor quality DS in which robust identification of emission features is difficult and 2 represents good data. All good dynamic spectra from different spacecraft are inspected and given an ‘event quality’ metric. This metric rates the quality of the event recorded. An event is rated along two axes: shape (S) and intensity (I). A type-II event with a well-discernible shape in the DS is given a rating of 3, while 1 represents an event whose shape is not very evident. This could be because it extends only within a narrow spectral band or because the event is in a crowded region of the DS where other burst types make the shape determination difficult. Similarly along the intensity axis, 3 represents a bright event while 1 denotes an event with a relatively low intensity in the region of the DS where it is detected. All dynamic spectra with a metric S_xI_y , where $x > 1$ and $y > 1$ are generally reliable. Of all the good dynamic spectra recorded for an event across spacecraft, the DS with the highest event quality metric identifies the observation line of sight that provided the best view of the event. The DS with the best event quality is used to estimate the L_R . The L_R was computed as the peak burst flux in the 3 - 7 MHz range. This frequency range was chosen because the type-III and type-II bursts are the major burst types in this range, and are relatively easily separable from one another due to their dynamic spectral morphology. Most long-duration broadband emission features that last for several hours to days, like the type-IV bursts are mostly confined above 7 MHz (Hillaris et al. 2016; Mohan et al. 2024). Hence in the higher frequency ranges often the type-II emission is mixed with type-IV bursts.

The aforementioned methodology led to a catalog of 163 DH type-II bursts with L_R estimates (hereafter ‘full catalog’). As discussed earlier, since the DS can have multiple co-temporal burst emission features occurring around similar frequency ranges we bestow a ‘reliability’ metric on the L_R estimate. Reliability metric rates L_R estimate along two axes: Field crowdedness (F) and relative flux (R). F quantifies how crowded the frequency-time field of the DS is where the type-II is observed. If there are other co-temporal emission features in the 3 - 7 MHz band intervening with the type-II emission, then F is given a high value. A value of 2 is given when the crowdedness is so high that the L_R is unreliable, while $F=1$ implies that L_R is reliable but the possibility of contamination from other emission features is

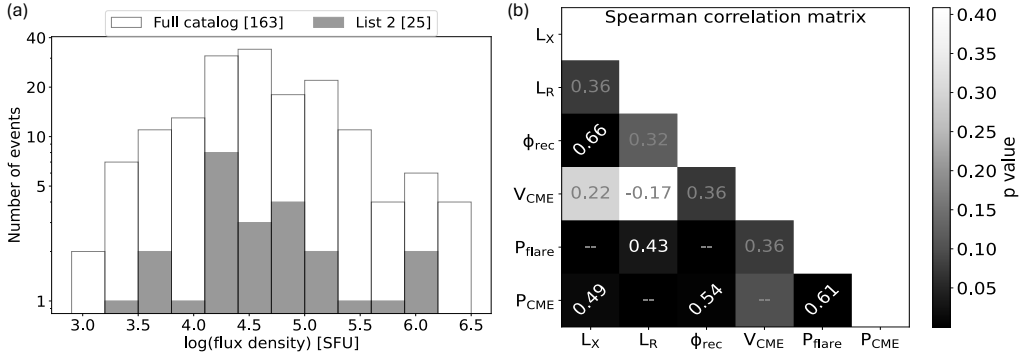


Figure 3. Statistical properties of the flare-CME-type-II events. (a): Flux density histogram. (b): Spearman correlation matrix for the various properties of the List 2 events. Numbers in each cell denote the correlation coefficient $C_{R,C}$ corresponding to the row (R) and column (C) parameters. Rotated text highlights strong correlations, white normal text denotes reliable weak $C_{R,C}$, and gray denotes the insignificant ones. Whenever R parameter is a function of C, $C_{R,C}$ is not mentioned.

non-negligible. 0 denotes the best case where the type-II is not close to any other radio emission feature and hence L_R is robust. Meanwhile, the relative flux (R) metric rates the flux level of the burst in the 3 – 7 MHz range in contrast to the typical burst flux outside of this chosen band. A value of 1 denotes that the 3 - 7 MHz flux is a good representative of the typical overall DH type-II burst flux level. A value of 0 would mean otherwise. So the FOR1 events have a very reliable L_R , which is also representative of the overall burst flux level.

For each event in the full catalog, L_X and V_{CME} were obtained by cross-matching the DH type-II event list with the catalogs maintained by the Coordinated Data Analysis Workshops (CDAW) group[†]. Events with good L_X and V_{CME} estimates were identified. Among those, the ones with an event quality S_xI_y , with $x,y \in 2,3$ and reliability (FOR1) were chosen and ϕ_{rec} was estimated using the post-eruption arcade method (Gopalswamy et al. 2018a). Finally, a list of 25 ‘flare-CME-type-II’ events (List 2) with reliable L_X, L_R, V_{CME} , and ϕ_{rec} estimates was produced that was used for further analysis. Figure 2 shows a portion of List 2. Peak_Flux provides radio flux density in 3 - 7 MHz band and F_thresh the mean background radio flux level. The time and frequency extents of the burst and the various quality metrics are also provided. The ‘CME’ section reports the maximum angular width and the speed of the interplanetary CME along with the time window of the event. Under the ‘Flare’ section, the location of the flaring active region as seen from the Earth (Src_loc), standard active region ID (NOAA), the peak SXR flux in the GOES scale[‡], ϕ_{rec} in Mx unit and absolute magnetic field strength at the flare region are provided. The link to the full catalog and event lists is in the caption of Fig. 2.

3. Results and discussion

Figure 3a shows the flux density distribution of the events in the full catalog and the sub-lists. A mean flux density of $\sim 3.5 \times 10^4$ SFU is found for all lists. Besides L_X, L_R, V_{CME} and ϕ_{rec} we define two new metrics of flare and CME power combining these quantities. The ‘flare power’,

[†] <https://cdaw.gsfc.nasa.gov/>

[‡] <https://www.swpc.noaa.gov/products/goes-x-ray-flux>

$P_{\text{flare}} = \sqrt{L_X \phi_{\text{rec}}}$, combines the strength in the magnetic reconnection with that in flare emissivity. Meanwhile the ‘CME power’, $P_{\text{CME}} = \sqrt{L_R V_{\text{CME}}^2}$, estimates the combined power in the CME kinetic energy that drives the shock and the associated particle acceleration. Figure 3b shows the result from the Spearman correlation analysis performed between parameter tuples drawn from the set comprising of L_R , L_X , ϕ_{rec} , V_{CME} , P_{flare} and P_{CME} . Each cell in the matrix plot shows the correlation coefficient ($C_{R,C}$) between the row (R) and column (C) parameter. The cell color represents the p-value. The significant strong $C_{R,C}$ are highlighted by slanting text ($C_{R,C} \gtrsim 0.49$ & $p < 0.015$). Straight white text represent reliable weak correlations ($C_{R,C} < 0.49$ & $p < 0.05$) and those in gray are insignificant ($p > 0.05$; $C_{R,C} < 0.49$). The correlation coefficients between tuples that are related by definition are masked and will not be considered in the analysis. After the well-known strongly correlated tuple (ϕ_{rec}, L_X) (Kazachenko et al. 2017; Sindhuja & Gopalswamy 2020), ($P_{\text{CME}}, P_{\text{flare}}$) is the strongly correlated pair with $C_{P_{\text{CME}}, P_{\text{flare}}} = 0.61$. The other strong correlations (green text) include (P_{CME}, L_X) and ($P_{\text{CME}}, \phi_{\text{rec}}$). Of all the strongly correlated parameter tuples where one parameter is fully flare-related and the other fully CME-related, ($P_{\text{CME}}, P_{\text{flare}}$) shows the highest $C_{R,C}$ value. Note that the individual terms that makeup P_{flare} and P_{CME} are not significantly correlated with each other, making the $P_{\text{flare}} - P_{\text{CME}}$ correlation robust. This correlation highlights the connection between the low-coronal and interplanetary particle acceleration events driven by the flare and the CME.

4. Conclusion

We present a catalog of decameter-hectometric (DH) type-II bursts with multi-vantage point observations from Wind and STEREO spacecraft. The data covers the interval from Nov 2006 to July 2023. Peak type-II flux in 3-7 MHz was found for all events along with the time-frequency extent of the burst. The full catalog has 163 events. For each type-II event, the catalog specifies the spacecraft that recorded the best view of the burst in terms of the time-frequency extent and morphology in the dynamic spectrum (DS). Also, the flare source location as seen from the Earth is mentioned. The DS of the best-viewed burst is rated along shape and intensity axes to help identify the events that demonstrated a well-characterizable shape with sufficient intensity. Along with the information on the source location and the relative position of the STEREO spacecraft, available from online resources[†] the catalog can be used to explore the line of sight dependency in the detection of radio bursts.

Cross-matching with the event catalogs compiled by the NASA-CDAW group, the properties of the associated soft X-ray (SXR) flare and interplanetary (IP) CME are compiled. The flare reconnection flux (ϕ_{rec}), peak SXR luminosity (L_X) and CME speed (V_{CME}) were either computed or compiled from existing catalogs, for all possible events. 25 events in the full catalog (List 2) had reliable estimates for $L_X, L_R, \phi_{\text{rec}}$ and V_{CME} . Using List 2 events, various correlations between flare, CME and type-II parameters were explored, to understand the interconnections, if any, between the particle acceleration processes in the low corona and IP space driven by the flare and the CME respectively. The newly defined flare and CME power terms, P_{flare} ($\sqrt{L_X \phi_{\text{rec}}}$) and P_{CME} ($\sqrt{L_R V_{\text{CME}}^2}$) respectively, demonstrate the highest correlation coefficient among all possible parameter tuples considered with one parameter purely flare-related and the other purely CME-related. The ϕ_{rec} and V_{CME} are also correlated with P_{CME} .

References

- Alvarado-Gómez, J. D., Drake, J. J., Cohen, O., et al. 2022, *AN*, 343, e10100
 Arzner, K. & Magun, A. 1999, *A&A*, 351, 1165
 Bastian, T. S. 1990, *Solar Phys.*, 130, 265
 Crosley, M. K. & Osten, R. A. 2018, *ApJ*, 856, 39

[†] https://stereo-ssc.nascom.nasa.gov/cgi-bin/make_where_gif

- Dulk, G. A., Gary, D. E., & Suzuki, S. 1980, *A&A*, 88, 218
- Gopalswamy, N. 2011, in *Planetary, Solar and Heliospheric Radio Emissions (PRE-VII)*, ed. H. O. Rucker, W. S. Kurth, P. Louarn, & G. Fischer, 325–342
- Gopalswamy, N., Akiyama, S., Yashiro, S., & Xie, H. 2018a, in Proc. IAU Symposium No. 335, ed. C. Foullon & O. E. Malandraki, Vol. 335, 258–262
- Gopalswamy, N., Akiyama, S., Yashiro, S., & Xie, H. 2018b, *Journal of Atmospheric and Solar-Terrestrial Physics*, 180, 35
- Gopalswamy, N., Mäkelä, P., & Yashiro, S. 2019, *Sun and Geosphere*, 14, 111
- Gopalswamy, N., Mäkelä, P., Yashiro, S., et al. 2018c, *ApJ (Letters)*, 868, L19
- Hillaris, A., Bouratzis, C., & Nindos, A. 2016, *Solar Phys.*, 291, 2049
- Howard, R. A., Vourlidas, A., & Stenborg, G. 2023, *FrASS*, 10, 1264226
- Kazachenko, M. D., Lynch, B. J., Welsch, B. T., & Sun, X. 2017, *ApJ*, 845, 49
- McLean, D. & Labrum, N. 1985, *Solar Radio Astrophysics* (Cambridge University Press)
- Miteva, R., Samwel, S. W., & Krupar, V. 2017, *JSWSC*, 7, A37
- Mohan, A., Gopalswamy, N., Kumari, A., Akiyama, S., & G, S. 2024, arXiv e-prints, arXiv:2406.00194
- Odert, P., Leitzinger, M., Guenther, E. W., & Heinzel, P. 2020, *MNRAS*, 494, 3766
- Osten, R. A. & Bastian, T. S. 2008, *ApJ*, 674, 1078
- Robinson, P. A. & Cairns, I. H. 1994, *Solar Phys.*, 154, 335
- Saint-Hilaire, P., Vilmer, N., & Kerdraon, A. 2013, *ApJ*, 762, 60
- Sindhuja, G. & Gopalswamy, N. 2020, *ApJ*, 889, 104
- Talebpour Sheshvan, N. & Pohjolainen, S. 2018, *Solar Phys.*, 293, 148
- Villadsen, J. & Hallinan, G. 2019, *ApJ*, 871, 214
- Wild, J. P. & McCready, L. L. 1950, *Australian Journal of Scientific Research A Physical Sciences*, 3, 387